

# Simulation of the effect of the laser beam profile on the overlap function of lidar systems

Nikolaos Siomos<sup>(a)</sup>, Michi Haimerl<sup>(a)</sup>, Volker Freudenthaler<sup>(a)</sup>

<sup>(a)</sup> Meteorologisches Institut, Ludwig-Maximilians-Universität München, Munich, Germany

[nikolaos.siomos@lmu.de](mailto:nikolaos.siomos@lmu.de)

**Abstract:** In order to get an estimation of its importance, we simulate the effect of the irradiance distribution of a laser beam on the overlap function of a lidar system. Five multi-modal and one Gaussian beam profiles were used and the overlap function was computed for each of them. We have calculated the errors, which are introduced to the lidar signals, while applying an overlap correction with a Gaussian beam profile instead of the actual one.

## 1. Introduction

Monitoring the first few hundred meters above ground can be challenging for most aerosol lidar systems. In the so-called near range, telescopes can detect only part of the backscattered radiation. This fraction also changes depending on the distance where scattering takes place. This region is known as the overlap region and the corresponding systematic effect is named overlap function. The overlap function is determined by multiple factors which originate both from the emitting (e.g. laser beam profile, laser-telescope alignment) and from the receiving part (e.g. telescope characteristics, field stop (FS) size and shape, acceptance angles of coatings, spatial homogeneity of the detector). In this study we focus on the effect of the laser beam profile on the overlap function by comparing the overlap function of different multi-modal beams, which exhibit extreme distinct spatial patterns in their intensity distribution, with the commonly assumed Gaussian beam.

## 2. Overlap simulator

In order to express the overlap function mathematically it is necessary to define a reference coordinate system (Fig. 1). Its center is the center of the primary mirror (PM) of the telescope. The  $z$  axis is perpendicular to the PM plane. The  $y$  axis points to the cross point of the laser beam with the  $xy$  plane, the so-called “north” direction. In our current application, we assume that the laser beam is emitted in the same plane as the PM and at distance  $y_{L,o}$ .

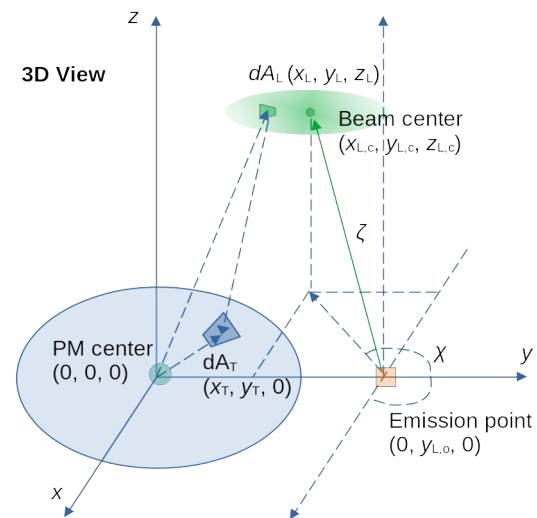


Figure 1: A 3D view of the laser beam (green) and the telescope primary mirror (PM) in the reference coordinate system

The emitted laser beam forms a zenith angle  $\zeta$  with the  $z$  axis, and its  $xy$  projection forms an azimuth angle  $\chi$  with the  $x$  axis. The center of the laser beam  $(x_{L,c}, y_{L,c}, z_{L,c})$  changes with  $z$ . The coordinates  $x_{L,c}, y_{L,c}$  are provided by Eqs. 1 and 2, respectively.

$$x_{L,c} = z_{L,c} \tan \zeta \cos \chi \quad (1)$$

$$y_{L,c} = y_{L,o} + z_{L,c} \tan \zeta \sin \chi \quad (2)$$

A single ray is defined as radiation coming from an infinitely small part  $dA_L$  of the laser beam that is transmitted through an infinitely small part of the telescope aperture  $dA_T$ . The coordinates  $x_L, y_L$  of  $dA_L$  in the reference system are given by Eqs. 3 and 4, respectively, where  $x_{L,w}$  and  $y_{L,w}$  are the  $x$  and  $y$  distances

from the center of the beam, respectively. The  $z$  coordinate is the same as  $z_{L,c}$ .

$$x_L = x_{L,c} + x_{L,w} \quad (3)$$

$$y_L = y_{L,c} + y_{L,w} \quad (4)$$

Rays transmitted through the aperture stop (here the PM) further propagate and finally reach the FS. We have made the following assumptions:

1. telescope aberrations are negligible
2. the FS is the limiting stop
3. spatial inhomogeneities in the transmission of the receiving optics are negligible
4. the effect of spatial inhomogeneities of the detector's sensitivity on the overlap function can be neglected
5. the effect of the angle of incidence of the rays on the transmission of the interference filters (IFs) can be neglected

The first assumption implies that the primary and the secondary mirror combined can be modeled as a thin lens. This is a safe assumption for most lidar system because the effect of aberrations is negligible compared to the divergence of the laser beam. The second assumption implies that rays that transmit through the FS are not truncated by any other stop of the system. This condition should be easily satisfied as it is usually the target at the manufacturing stage. The third assumption can be fulfilled by careful selection of optical elements with high quality. The transmission is expected to be homogeneous for high quality optics. The validity of the fourth assumption is difficult to check as the inhomogeneities of the detector are seldom known. Such effects are minimized for systems which create an image of the PM (aperture stop) on the detector surface. The fifth assumption can be fulfilled by using IFs with sufficiently broad bandwidth.

A schematic showing a ray being transmitted through the FS can be seen in Fig. 2. The FS is a circular diaphragm perpendicular to the  $z$  axis. Its center can be displaced by  $\Delta x_{FS,o}$ ,  $\Delta y_{FS,o}$ , and  $\Delta z_{FS,o}$  with respect to the focal point. Rays that pass through the FS must fulfill Eq. 5.

$$(x_{FS} - \Delta x_{FS,o})^2 + (y_{FS} - \Delta y_{FS,o})^2 \leq \left(\frac{D_{FS}}{2}\right)^2 \quad (5)$$

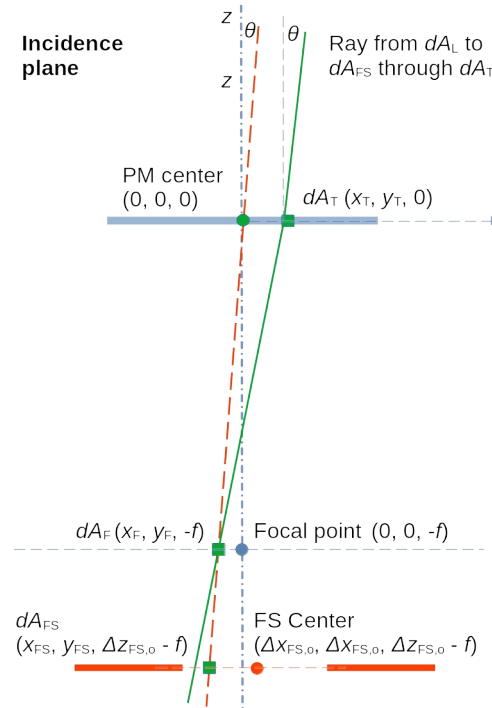


Figure 2: Transmission of a ray through the primary mirror (PM) and the field stop (FS).

Here  $x_{FS}$  and  $y_{FS}$  correspond to the coordinates of surface  $dA_{FS}$  at which the ray crosses the FS plane and are provided by Eqs. 6 and 7, respectively.

$$x_{FS} = \frac{x_T - x_L}{z_L} (f - \Delta z_{FS,o}) + x_T \frac{\Delta z_{FS,o}}{f} \quad (6)$$

$$y_{FS} = \frac{y_T - y_L}{z_L} (f - \Delta z_{FS,o}) + y_T \frac{\Delta z_{FS,o}}{f} \quad (7)$$

The signal  $dS_T$  which is collected when a ray reaches the detector surface is given by Eq. 8.

$$dS_T = \frac{\eta T_o f_{FS} f_T T_{A,o}(z) \beta_s(z) T_{A,s}(z) E_L dA_T dA_L}{z^2} \quad (8)$$

Here  $E_L(x_L, y_L, z_L)$  is the irradiance (flux density) of the divergent laser pulse (in  $W m^{-2}$ ),  $T_{A,o}(z)$  and  $T_{A,s}(z)$  are the atmospheric transmission at the emitted and scattered wavelengths  $\lambda_o$  and  $\lambda_s$ , respectively,  $\beta_s(z)$  is the atmospheric backscatter coefficient at  $\lambda_s$ , and  $f_T(x_T, y_T)$  is a function that describes partial or complete shadowing of any parts before the PM aperture, ranging from 0 (total obscuration) to 1 (no obscuration). The

truncation of rays by the FS is expressed by the  $f_{FS}(x_L, y_L, x_T, y_T)$  term which can be 0 or 1 for total or no obscuration, respectively. Finally, the total transmission of the optics is included with the constant term  $T_O$  and the detector gain is provided by the constant  $\eta$  term.

The total signal collected by the detector can be calculated by integrating over the PM aperture and over the laser beam at a specific range  $z$ . The overlap function of the system includes all terms that vary along  $x$  and  $y$  with range  $z$  and is given by Eq 9:

$$O(z) = \iint_{A_L} \iint_{A_T} f_{FS} f_T E_L dA_T dA_L \quad (9)$$

We have assumed here that the atmospheric scatterers are homogeneously distributed across the  $xy$  plane for every height. We can also assume that  $xy$  cross sections of the beam are equivalent to transverse cross section because  $\zeta$  is on the order of a few mili-radians for lidar applications.

### 3. Simulating the laser beam

A common representation of a laser beam is a 2D Gaussian irradiance distribution. In practice, the actual energy distribution changes from pulse to pulse. Averaging over many pulses, which is a common practice in most aerosol lidar applications, should smooth out those temporal shot-by-shot fluctuations. The mean distribution shape, though, can still divert significantly from the ideal Gaussian shape. Examples of real far range cross sections of laser beams in lidar systems can be seen in Fig 3.

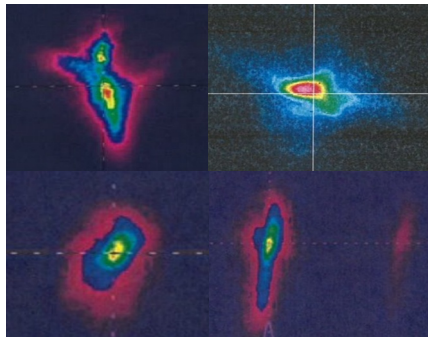


Figure 3: Examples of multi-modal beams in the far range.

According to Eq. 9, the beam irradiance distribution affects the overlap function of the system. In this study we focus on the

uncertainties introduced to the overlap function by assuming a Gaussian beam profile instead of a more complex multi-modal beam profile.

Any coherent beam can be simulated as a linear combination of transverse electromagnetic modes (TEM), each weighted with a specific amplitude and shifted by a specific phase (see e.g. [1]). We have used Hermite-Gaussian modes up to 3<sup>rd</sup> order to simulate far range beams of distinct characteristic shapes. Multi-modal beams change between the near and the far field ( $\sim \pm 3$  times the Rayleigh length). The Rayleigh length is typically on the order of a few meters and the far field is reached in less than 10 m, which is too low to play a role in our overlap simulations. Consequently, we have considered only far field modes that have acquired their respective Gouy phase in the far range [2]. No additional phase shift is introduced (e.g. due to interaction with the emission optics). The modes' amplitudes are weighted in order to achieve the desired degree of irregularity.

### 4. Results

The receiver in our simulations includes a telescope with a focal length  $f$  of 1 m and a diameter  $D_T$  of 200 mm. The center of the FS is displaced in the  $z$  direction by  $\Delta z_{FS,o} = -2$  mm with respect to the focal point. Its diameter  $D_{FS}$  is 1 mm. The laser beam is emitted parallel to the  $z$  axis ( $\zeta = 0, \chi = 0$ ) and the laser-telescope-axes distance  $y_{L,o}$  is 180 mm.

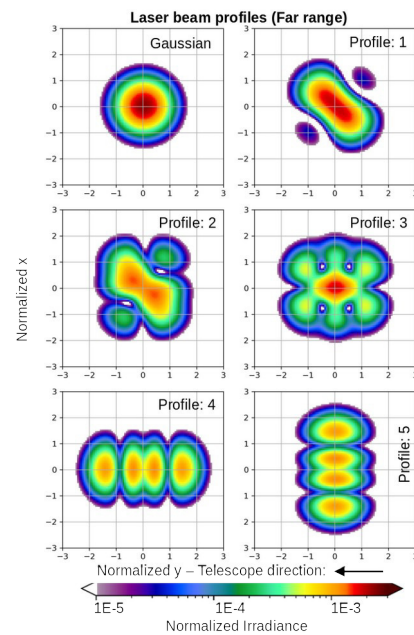


Figure 4: Six simulated far range beam profiles

We have simulated six beam profiles in the far range, one of which is Gaussian and the rest (1 to 5) are multi-modal beams (see Fig. 4). The irradiance  $E_L$  is normalized so that the integral (radiant flux) of the whole profile over the x and y axis is 1 W. The color-scale is logarithmic. The beam profiles are scaled so that their divergence, defined as the angle of a circular cone that includes 98.9% of the radiant flux of the beam, is the same as the 3-sigma divergence of a Gaussian beam.

We use Eq. 9 to calculate the overlap function for each beam profile. Then, we compute the relative difference of the overlap function of the Gaussian profile from each other profile. This difference is the relative systematic error introduced on a signal when an overlap correction is applied assuming a Gaussian beam instead of the actual beam.

The overlap functions for all multi-modal beams are presented in Fig. 5. The absolute differences from the Gaussian are highest between 400 and 600 m. The distance of full overlap, defined as the distance where the overlap function becomes 0.95, ranges between 445 m for the 4<sup>th</sup> and 525 m for the 5<sup>th</sup> profile.

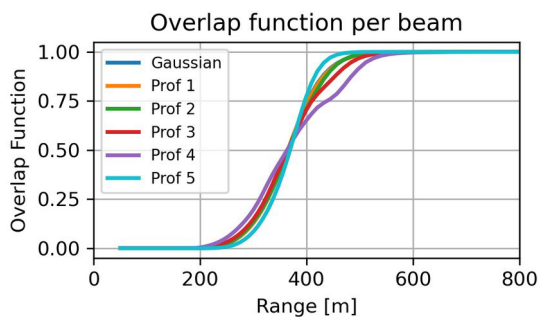


Figure 5: The overlap functions of the simulated beam profiles of fig. 4 with the lidar receiver described in the text.

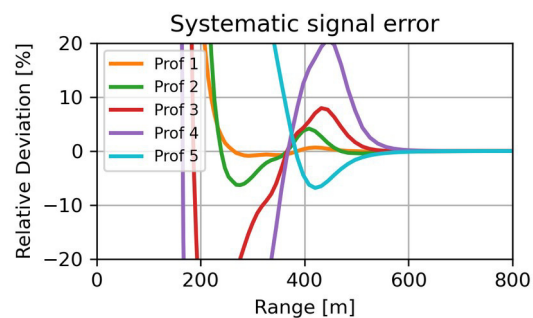


Figure 6: Systematic signal error assuming a Gaussian beam for the overlap correction

The relative deviations of the signals can be seen in Fig. 6. It is obvious that an overlap correction assuming a Gaussian beam profile is already meaningless below 350 m for the 3<sup>rd</sup>, 4<sup>th</sup>, and 5<sup>th</sup> profiles as the introduced relative errors become much larger than 20%. We will, therefore, focus only on ranges above 350 m.

The highest relative errors, which go up to 20%, are observed for the 4<sup>th</sup> profile, probably because it is the one with the highest divergence on the y axis (north – south direction). The errors are less than 8% for the other profiles. The 1<sup>st</sup> profile shows almost no difference compared with the Gaussian. The 2<sup>nd</sup>, 3<sup>rd</sup>, and 4<sup>th</sup> profiles show similar deviation patterns. In contrast with the other profiles, the 5<sup>th</sup> one shows a different, almost anti-correlated, pattern. This is probably because it is more divergent on the x axis. It also seems that complex structures, e.g. gaps in the irradiance profile, are not primarily determining the overlap function because the 2<sup>nd</sup> and 3<sup>rd</sup> profiles, that have the most complex shapes, do not introduce the largest differences. It is possible that these differences are mainly driven by the different divergence of the beams along the x and y axis. In the future, we will investigate in which extent an elliptical beam profile can be a better approximation that reproduces the overlap function of more complex profiles with the same elliptical characteristics sufficiently.

## 5. Acknowledgments

This project/ receives funding from the European Union’s Horizon 2020 research and innovation programme under grant agreements No 871115. ACTRIS-D is funded by the German Federal Ministry for Education and Research (BMBF) under grant agreements 01LK2001A-K & 01LK2002A-G.

## 6. References

- [1] O. A. Schmidt *et al.*, “Real-time determination of laser beam quality by modal decomposition,” *Opt. Express*, vol. 19, no. 7, pp. 6741–6748, Mar. 2011, doi: 10.1364/OE.19.006741.
- [2] O. Svelto, *Principles of Lasers*. Boston, MA: Springer US, 2010. doi: 10.1007/978-1-4419-1302-9.